# Attractor dynamics of a Boolean model of a brain circuit controlled by multiple parameters

Jérémie Cabessa, and Alessandro E. P. Villa

Citation: Chaos **28**, 106318 (2018); doi: 10.1063/1.5042312
View online: https://doi.org/10.1063/1.5042312
View Table of Contents: http://aip.scitation.org/toc/cha/28/10
Published by the American Institute of Physics

# Attractor dynamics of a Boolean model of a brain circuit controlled by multiple parameters

Jérémie Cabessa[1,a)] and Alessandro E. P. Villa[2,b)]
[1]*Laboratory of Mathematical Economics (LEMMA), Université Paris 2—Panthéon-Assas, 75005 Paris, France*
[2]*Neuroheuristic Research Group, University of Lausanne, CH-1015 Lausanne, Switzerland*

(Received 31 May 2018; accepted 29 August 2018; published online 18 October 2018)

Studies of Boolean recurrent neural networks are briefly introduced with an emphasis on the attractor dynamics determined by the sequence of distinct attractors observed in the limit cycles. We apply this framework to a simplified model of the basal ganglia-thalamocortical circuit where each brain area is represented by a "neuronal" node in a directed graph. Control parameters ranging from neuronal excitability that affects all cells to targeted local connections modified by a new adaptive plasticity rule, and the regulation of the interactive feedback affecting the external input stream of information, allow the network dynamics to switch between stable domains delimited by highly discontinuous boundaries and reach very high levels of complexity with specific configurations. The significance of this approach with regard to brain circuit studies is briefly discussed. *Published by AIP Publishing.*
https://doi.org/10.1063/1.5042312

**Boolean recurrent neural networks offer the advantage to study the computational and dynamical features of biological neural networks in a simplified, yet formally defined framework. The attractors of such networks correspond precisely to the cycles in the graphs of their corresponding automata and can thus be computed explicitly and exhaustively. The basal ganglia-thalamocortical circuit is among the most important brain circuit to make a bridge between perceptual, cognitive, emotional, and decision-making information processing. We study its attractor dynamics by means of a Boolean model that allows an evaluation of important computational features. The complexity of the dynamics of this model is determined by both the number and the stability of the attractors encountered throughout the computational process. We show that control parameters such as neuronal excitability and fine tuning of the connection strengths can settle the network activity into stable attractor dynamics delimited by highly discontinuous boundaries. A feedback regulation of the external input stream may, to some extent, combine and compensate with the other control parameters in order to increase the complexity and stabilize the attractor dynamics. We introduce a biologically plausible adaptive plasticity rule, which modifies the connection strengths as a function of the attractor dynamics encountered throughout the computational process, in addition to the timing between the activations of pre- and post-synaptic neurons. This rule sets the basis for the network to reach and stabilize into attractor dynamics of high complexity. We conclude with a discussion about the significance of this framework for the investigation of the functions of brain circuit modeled by Boolean recurrent networks, in particular for the basal ganglia-thalamocortical circuit.**

[a)]Electronic mail: jeremie.cabessa@u-paris2.fr
[b)]Electronic mail: alessandro.villa@unil.ch

## I. INTRODUCTION

Neurons are excitable cells whose activity may be described by highly nonlinear dynamical equations determined by the biophysical properties of the cell membrane and by molecular and cellular reactions.[1] Neuronal activity is characterized by sensitivity to timing of changes in the cellular electrochemical environment.[2,3] Experimental evidence exists of spatiotemporal patterns of neuronal discharges—the spikes—, also referred to as preferred firing sequences, that correspond to repeated ordered and precise interspike interval relationships which recur above chance levels.[4–8] A detailed analysis of the spike trains—the time series formed by the neuronal discharges—revealed the presence of deterministic chaotic attractors in experimental recordings.[9–12] Evidence provided by the analysis of electroencephalogram (EEG) recordings also supports the hypothesis of the existence of deterministic dynamics in brain activity.[13,14] An association between spatiotemporal firing patterns and chaotic attractor dynamics was observed in theoretical[15] and large scale neuronal network simulations with embedded neurodevelopmental features.[16] In other words, the spatiotemporal patterns would be the witnesses of the capacity of neural systems to converge to particular invariant states of network activity referred to as *attractor states*.

Stability in the face of continuous perturbations is a hallmark of attractor dynamics[17]. It is required for persistence of function associated with any form of neural coding.[18,19] In information theory, the term *coding* refers to a substitution scheme where the message to be encoded is replaced by a special set of symbols. However, substitution codes are essentially static and seem unlikely to exist in the nervous system. Time sequences, delays, and precise coincidence relationships are critically important aspects of neural information processing, and the possibility to fit them into substitution codes appears rather remote. On the contrary, *attractors* defined by sequences of states determined by the network dynamics are a valuable metaphor for dynamical coding schemes.

In this conceptual framework, meaningful attractors are associated with memory and motor patterns and spurious attractors associated with stable activity states not explicitly encoded in the network.[19–22]

Attractor theory of neural information processing necessarily requires precise time coding, as observed experimentally.[4–8,23] Other experimental evidence based on a direct transfer function between stimulus and response intensities[24,25] assumes that the rate, and not the timing, of neuronal discharges contains most, if not all, of the information exchanged throughout a neural network.[26] This assumption led to the mainstream framework of artificial neural networks characterized by analog elements that transmit and process information based on scalar values produced as neuronal outputs.[27–29] It is interesting to remark that rate and temporal coding can be reconciled to some extent because, at the appropriate timescales, neuronal spike trains may be compared to binary streams where each neuron gives at most one spike per bin.[30] Therefore, the state of each neuron can be described by a binary variable, and neural networks can be approximated by Boolean recurrent neural networks.

The framework of Boolean networks, although relatively simple, has the advantage of allowing for a complete analysis of the attractor dynamics of the networks. The attractors of the Boolean networks correspond precisely to the cycles in the graphs of their corresponding automata and can thus be computed explicitly and exhaustively.[31,32] The theoretical study of the expressive capabilities and the computational power of recurrent neural networks can be studied from the perspective of their attractor dynamics.[32–38] Accordingly, a novel *attractor-based measure of complexity* for Boolean recurrent neural networks based on the graph theoretic complexity of their corresponding automata has been introduced.[32] This complexity measure is primarily related to the dynamics and is associated with the ability of the networks to perform more or less complicated classification tasks via the expression of meaningful or spurious attractor dynamics. The network structure strongly influences the dynamics of neural networks, and the flexibility offered by tuning the dynamical properties of the network is an essential feature of natural systems to shift among the attractors following contextual needs. For instance, in the real world, most activities of neural systems are transient, and signal-dependent transitions in the state space must be reliably driven by the network dynamics. Extensive studies in globally coupled maps and neural networks[39–42] demonstrated the switching of attractors just by adding noise, and the selection of an attractor triggered by external stimuli may be considered as recall of a memory.[20,21,43,44] More generally, itinerancy between attractors including infinitely many unstable periodic orbits can be associated with transitions in a chaotic multistable neural system according to interactivity between internal dynamics and perceptual information.[45–47]

The connection strengths—synaptic weights—between the neurons play a key role both in the computational power of neural networks as well as in the emergence and stability of specific patterns of activity. From a purely computational perspective, integer-weighted neural networks are computationally equivalent to finite state automata and rational-weighted neural networks are equivalent to deterministic Turing machines, whereas all other models of real-weighted or evolving neural networks are equivalent to each other and strictly more powerful than Turing machines (super-Turing).[34,35,38,48–50] From a dynamical perspective, a self-organization of the synaptic-weight matrix may be initially required to form stable attractors, but relative weightings based on dynamic conditions determined by learning any kind of perceptual information is necessary to define specific neural functions.[51–54] Persistence of coexistent synchronization patterns regardless of the initial conditions is promoted by increasing the heterogeneous distribution of coupling weights in the neural networks.[55]

In this paper, we investigate the complexity in attractor dynamics of a Boolean model of the basal ganglia-thalamocortical network.[32] We present evidence that small changes in control parameters such as neuronal excitability and connection strengths can increase and stabilize the complexity of attractor dynamics. We also show that feedback regulation of the external inputs may, to some extent, combine and compensate with the other control parameters in order to settle the network dynamics into stable domains of high complexity. In addition, we introduce an adaptive *spike-timing dependent plasticity* (*STDP* rule[56–58]) associated with increasing levels of complexity of the attractor dynamics. This new STDP rule modifies the connection strengths as a function of the attractor dynamics encountered throughout the computational process, in addition to the timing between the activations of pre- and post-synaptic neurons. We show that this rule brings the network activity to reach and stabilize into attractor dynamics of high complexity. Our results demonstrate that finely tuned and targeted changes in selected synapses may dramatically increase the attractor complexity of neural network dynamics. We conclude with a discussion of the outcome of this rule on the function of the basal ganglia-thalamocortical network.

## II. BOOLEAN RECURRENT NEURAL NETWORKS

We briefly introduce our framework of Boolean recurrent neural networks, as defined and previously developed elsewhere.[32,59] A *first-order Boolean recurrent neural network* (*RNN*) consists, in a formal definition, of a synchronous network $\mathcal{N}$ of interconnected neurons composed of $M$ Boolean input neurons $(u_k)_{k=1}^{M}$ and $N$ Boolean internal neurons $(x_i)_{i=1}^{N}$ [Fig. 1(a)]. The dynamics of the network is computed as follows: given the activation values of the input and internal neurons $[u_k(t)]_{k=1}^{M}$ and $[x_j(t)]_{j=1}^{N}$ at time $t$, the activation values of the internal neurons $[x_i(t+1)]_{i=1}^{N}$ at time $t+1$ are computed as

$$x_i(t+1) = f_\theta\left[\sum_{j=1}^{N} a_{ij}\cdot x_j(t) + \sum_{k=1}^{M} b_{ik}\cdot u_k(t) + c_i\right], \quad (1)$$

for $i = 1,\ldots,N$, where $a_{ij}$ and $b_{ik}$ are the values of the connection strengths—or *synaptic weights*—from internal neuron $j$ to internal neuron $i$ and from input neuron $k$ to internal neuron $i$, respectively, $c_i$ is the *bias* of cell $x_i$, $\theta$ is the *threshold* of excitability (being the same for all neurons and equal to 1

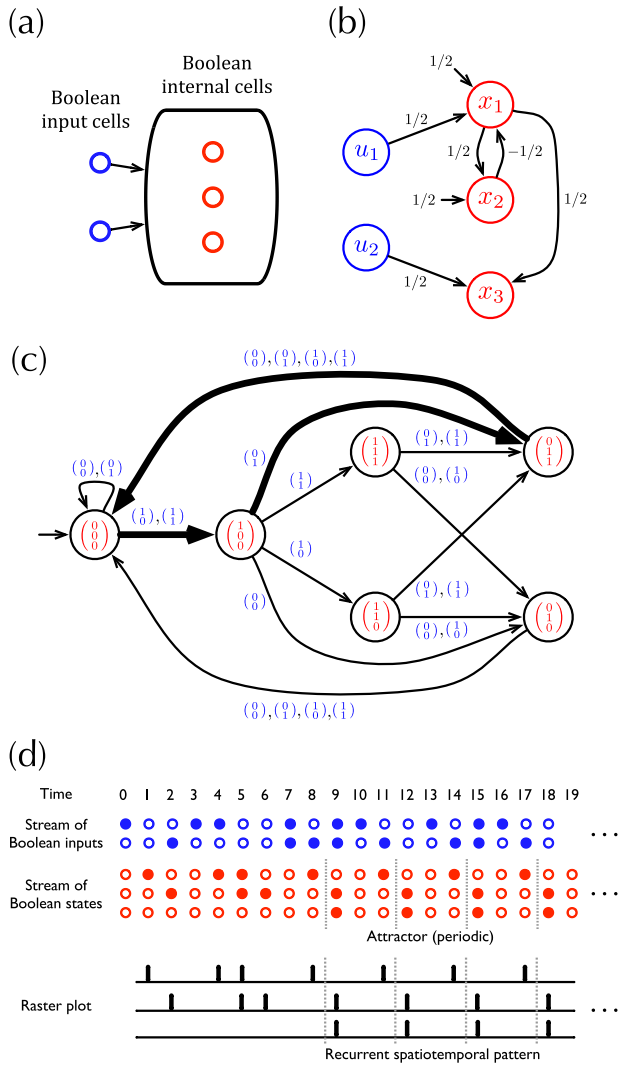


FIG. 1. (a) A general Boolean neural network. (b) A simple first-order Boolean recurrent neural network with two input neurons $u_1$ and $u_2$ and three internal neurons $x_1$, $x_2$, and $x_3$. (c) The finite automaton $\mathcal{A}$ associated with the Boolean recurrent neural network $\mathcal{N}$. The nodes of $\mathcal{A}$ are the states of $\mathcal{N}$, and there is an edge from node $\vec{s}_i$ to node $\vec{s}_j$ labelled by $\vec{u}$ if and only if network $\mathcal{N}$ switches from state $\vec{s}_i$ to state $\vec{s}_j$ when receiving $\vec{u}$. According to this construction, the cycles in the graph of $\mathcal{A}$ correspond precisely to the attractors of $\mathcal{N}$. For instance, the boldface cycle corresponds to the attractor $\{(0,0,0)^T, (1,0,0)^T, (0,1,1)^T\}$. (d) Dynamics of this Boolean network. The boldface cycle above is generated by the Boolean input stream (blue dots) falling into a specific sequence of Boolean states (red dots) corresponding to an attractor dynamics (indicated by the dashed lines). Whenever the attractor occurs in the network dynamics, a recurrent spatiotemporal pattern of activity is observed in the firing sequence of the internal neurons.

unless specified), and $f_\theta$ is the hard-threshold activation function given by $f_\theta(x) = 1$ if $x \geq \theta$ (meaning that the neuron is spiking), and $f_\theta(x) = 0$ if $x < \theta$ (meaning that the neuron is quiet).

According to Eq. (1), the dynamics of the whole network $\mathcal{N}$ is described by the equation

$$\vec{x}(t+1) = f_\theta\left[A \cdot \vec{x}(t) + B \cdot \vec{u}(t) + \vec{c}\right], \tag{2}$$

where $A = (a_{ij})$, $B = (b_{ij})$, and $\vec{c} = (c_i)$ are the two weight matrices and bias vector, respectively, $\vec{x}(t) = [x_1(t), \ldots, x_N(t)]$ and $\vec{u}(t) = [u_1(t), \ldots, u_M(t)]$ are the Boolean vectors—or *Boolean state*—describing the spiking configuration of the internal and input neurons at time $t$, and $f_\theta$ denotes the hard-threshold function applied to each element of the network. An example of a simple (*RNN*) is given in Fig. 1(b).

### A. Correspondence with finite state automata

Boolean recurrent neural networks are computationally equivalent to finite state automata.[48,49] For any Boolean network $\mathcal{N}$, its corresponding automaton $\mathcal{A}$ can be constructed as follows: the nodes of $\mathcal{A}$ correspond to the states of $\mathcal{N}$, and there is an edge from node $\vec{s}_i$ to $\vec{s}_j$ labelled by $\vec{u}$ in $\mathcal{A}$ if and only if $\mathcal{N}$ moves from the Boolean state $\vec{s}_i$ to $\vec{s}_j$ when receiving the Boolean input $\vec{u}$. Note that if $\mathcal{N}$ contains $N$ internal cells, then it can disclose up to $2^N$ possible states. Thus, $\mathcal{A}$ contains at most $2^N$ nodes. According to this construction, the various *dynamics* of network $\mathcal{N}$ correspond precisely to the different *paths* in the graph of automaton $\mathcal{A}$. Indeed, the successive Boolean states forming a particular dynamics of $\mathcal{N}$ are represented by successive nodes along a corresponding path in the graph of $\mathcal{A}$. As a consequence, the cyclic dynamics—i.e., the *attractors*—of $\mathcal{N}$ corresponds precisely to the cyclic paths—i.e., the *cycles*—in the graph of $\mathcal{A}$.[32] Therefore, it suffices to construct the associated automaton $\mathcal{A}$ and list all the cycles of this latter in order to compute the attractors of a network $\mathcal{N}$. Formally, an attractor of a Boolean network $\mathcal{N}$ is a set of Boolean states $X = \{\vec{x}_0, \ldots, \vec{x}_k\} \subseteq \mathbb{B}^N$ such that, for some infinite input stream, the dynamics of $\mathcal{N}$ visits infinitely often every state of $X$ and no other ones from some time step onwards. These attractors can thus be computed exhaustively.

A simple Boolean recurrent neural network and its corresponding finite state automaton are illustrated in Figs. 1(b) and 1(c). The nodes of the automaton are the Boolean states of the network that are reachable from the initial state $\vec{0}$. The edges of the automaton correspond to the transitions between those states and are labelled by the Boolean inputs of the network. As an example, suppose that this network is receiving the following infinite periodic input stream (where the "$\omega$ exponent" means that the pattern is repeated *ad infinitum*)

$$\left[\begin{pmatrix}0\\1\end{pmatrix}\begin{pmatrix}1\\1\end{pmatrix}\begin{pmatrix}1\\0\end{pmatrix}\begin{pmatrix}0\\1\end{pmatrix}\begin{pmatrix}0\\0\end{pmatrix}\begin{pmatrix}1\\0\end{pmatrix}\right]^\omega.$$

Then, according to Eq. (2), the network will produce the corresponding infinite sequence of Boolean states

$$\underset{t=0}{\begin{pmatrix}0\\0\\0\end{pmatrix}} \cdots \underset{\substack{t=9,\ t=10,\ t=11\\ t=12,\ t=13,\ t=14\\ t=15,\ \ldots}}{\left[\begin{pmatrix}0\\1\\1\end{pmatrix}\begin{pmatrix}0\\0\\0\end{pmatrix}\begin{pmatrix}1\\0\\0\end{pmatrix}\right]^\omega}.$$

This dynamics corresponds to the following path in the automaton of Fig. 1(c):

$$\begin{pmatrix}0\\0\\0\end{pmatrix} \xrightarrow{\binom{0}{1}} \cdots \xrightarrow{\binom{1}{0}} \begin{pmatrix}0\\1\\1\end{pmatrix} \xrightarrow{\binom{0}{1}} \begin{pmatrix}0\\0\\0\end{pmatrix} \xrightarrow{\binom{0}{0}} \begin{pmatrix}1\\0\\0\end{pmatrix} \xrightarrow{\binom{1}{0}} \cdots.$$

In this case, note that the set of states $X = \{(0,1,1)^T, (0,0,0)^T, (1,0,0)^T\}$ is an attractor, because the network dynamics remains confined into it from time step 9 onwards. This attractor corresponds to the cycle $[(0,0,0)^T, (1,0,0)^T, (0,1,1)^T,$

$(0,0,0)^T$] depicted in boldface in the automaton of Fig. 1(c). In this automaton, we can list all simple cycles and deduce that the network of Fig. 1(b) is characterized by 7 attractors, which are as follows:

$$\{(0,0,0)^T\}$$
$$\{(0,0,0)^T, (1,0,0)^T, (0,1,1)^T\}$$
$$\{(0,0,0)^T, (1,0,0)^T, (1,1,1)^T, (0,1,1)^T\}$$
$$\{(0,0,0)^T, (1,0,0)^T, (1,1,1)^T, (0,1,0)^T\}$$
$$\{(0,0,0)^T, (1,0,0)^T, (1,1,0)^T, (0,1,1)^T\}$$
$$\{(0,0,0)^T, (1,0,0)^T, (1,1,0)^T, (0,1,0)^T\}$$
$$\{(0,0,0)^T, (1,0,0)^T, (0,1,0)^T\}.$$

Any Boolean recurrent neural network $\mathcal{N}$ is always formed by finitely many internal cells, and then it comprises finitely many possible Boolean states. Therefore, any of its infinite dynamics will eventually get trapped into some set of states that repeat infinitely often, namely, into some attractor (indeed, any infinite sequence of finitely many possible elements begins to repeat from some point onwards, but not necessarily in a periodic way). Note that if the dynamics of the network gets trapped into an attractor, then the raster plot of any subset of the internal cells would necessarily reveal a preferred firing sequence corresponding to some *recurrent spatiotemporal patterns* of spikes repeating more often than expected by chance. Therefore, in this framework, the spatiotemporal patterns of activity are precise witnesses of an underlying attractor dynamics. In the example of Fig. 1(d), the network dynamics gets trapped into the attractor $X = \{(0,1,1)^T, (0,0,0)^T, (1,0,0)^T\}$, and a precise spatiotemporal pattern of activity (i.e., a repeating stream of Boolean states) is a witness of that attractor. Any other infinite dynamics, periodic or not, would also get trapped, after some time, into one or many of the 7 attractors and generate the corresponding spatiotemporal patterns of activity.

It is important to note that the entire list of attractors belonging to a network dynamics can be fully determined at any time step by knowing the set of variables defining the topology of a network—i.e., the number and the kind of cells, the connectivity pattern—and the set of control parameters—e.g., the threshold of excitability of each cell, the time constants of the cell membrane, the refractory period, etc. Hence, in the absence of any external force or rule affecting the network—e.g., death of cell or cell multiplication, pruning or growing synaptic connections, synaptic plasticity, adaptive threshold of excitability, dynamic changes in resistivity, and capacitance of cell membrane—the attractors do not change, irrespective of the input pattern. However, any modification of the network's topology and control parameters induces a modification of its attractors, and at any time step, it is necessary to recompute the list of attractors if one wants to know a measure of the complexity of the network dynamics.

### B. Measure of complexity based on network dynamics

On the basis of neurophysiological criteria, it is possible to evaluate the meaningfulness of an attractor (i.e., the meaningfulness of a recurrent pattern of activity), and the simplest categorization assumes that any attractor of a network can be classified into two possible types: meaningful or spurious. An *attractor-based measure of complexity* for Boolean recurrent neural networks is given by a graph theoretic analysis of the meaningful and spurious cycles contained in its corresponding automaton.[32] The specificity of this complexity measure is that it is primarily related to the dynamics rather than to the topology of the networks, and it is associated with the ability of the networks to perform more or less complicated classification tasks. In this paper, in order to avoid the evaluation necessary for any categorization of the meaningfulness of the attractors, we consider the *number of attractors* associated with the Boolean networks as a representative, yet simpler, measure of the complexity of network dynamics.

## III. BOOLEAN MODEL OF THE BASAL GANGLIA-THALAMOCORTICAL NETWORK

### A. Functionality and relevance of the network components

The basal ganglia-thalamocortical network is formed by several parallel and segregated circuits involving different areas of the cerebral cortex, striatum, pallidum, thalamus, subthalamic nucleus, and midbrain.[60] In the basal ganglia, we considered the circuit including the two so-called "direct" striatonigral and "indirect" striatopallidal inhibitory pathways. The inhibitory GABAergic striatal neurons (Str) expressing the dopamine D1 receptors (Str-D1) projects to the substantia nigra pars reticulata (Snr) and pallidum (internal segment, GPi, and external segment, GPe). Those neurons expressing mainly the dopamine D2 receptors (Str-D2) project almost exclusively to the external pallidal segment (GPe). However, recent investigations suggested that a subpopulation of striatal neurons coexpressing both D1 and D2 receptors might be considered as the source of a third and separate neuronal pathway with putative distinct signalling functions.[61] In the current model, we considered only the two main striatonigral and striatopallidal inhibitory projections. The external pallidal segment (GPe) is a real hub, with the majority of its neurons being GABAergic and sending projections mainly to other basal ganglia nuclei including the striatum, GPi/Snr, the subthalamic nucleus (STN), and to the thalamic reticular nucleus (NRT). The subthalamic nucleus (STN) is the main source of excitatory projections within the basal ganglia, in particular to GPe, GPi, SNr and is reciprocally connected with excitatory connections with the cerebral cortex.[62]

The main output structure of the basal ganglia is represented by the substantia nigra pars reticulata (Snr) and the pallidal internal segment (GPi), whose GABAergic inhibitory projections reach the central and dorsal thalamic nuclei (Thalamus) and the midbrain (e.g., the superior colliculus, SC). The overall characteristic of the basal ganglia-thalamocortical network is a combination of "open" and "closed" loops with ascending sensory afferences reaching the thalamus and the midbrain, as well as with descending motor efferences from the midbrain (the tectospinal tract) and the cortex (the corticospinal tract). Fig. 2(a) shows a sketch of the network considered in this study. Notice the presence of chains of polysynaptic inhibitory connections, such as GPe → Str → GPe → GPi/SNr → NRT → Thalamus. Further details

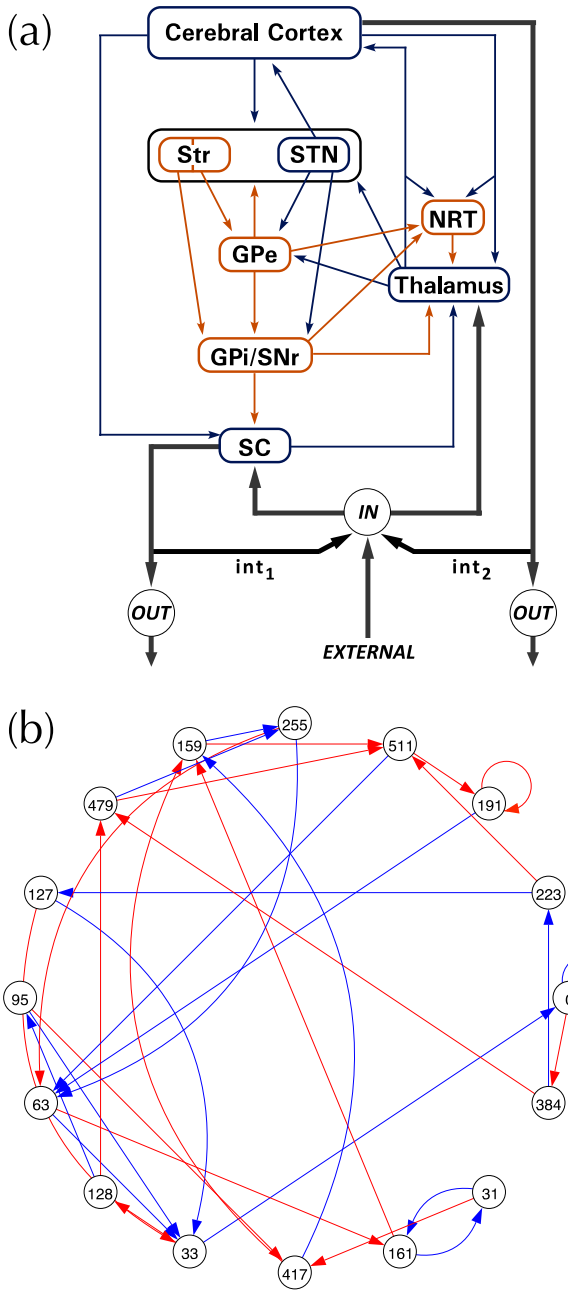


FIG. 2. (a) Boolean model of the basal ganglia-thalamocortical network constituting 9 different interconnected brain areas, each one represented by a single node in the model.[32] Dark blue or orange arrows correspond to positive and negative weights, respectively. Notice the recurrent connections $\text{int}_1$ and $\text{int}_2$, which will be referred to as the *interactive connections*. (b) Finite state automaton associated with the network of panel (a). Each node of the automaton is a Boolean state of the network. Blue or red edges correspond to transitions from state $i$ to state $j$ when receiving input 0 or 1, respectively. The cycles in the automaton correspond to the attractors of the network.

regarding the connections of this circuit have been discussed elsewhere.[32]

Here, we assume that each brain area is modeled by a Boolean node; thus, the whole brain circuit is modeled by a Boolean neural network composed of 9 nodes [Fig. 2(a)] with its adjacency matrix given in Table I. The threshold of excitability for all nodes is assumed to be equal to 1 (unless specified). Each node of the automaton represents a Boolean state of the network. Each Boolean state is defined according

TABLE I. Adjacency matrix of the Boolean model of the basal ganglia-thalamocortical network (Fig. 2).

| **Source** | | **Target** node# | | | | | | | | | |
|---|---|---|---|---|---|---|---|---|---|---|---|
| Node# | Name | 0 | 1 | 2 | 3 | 4 | 5 | 6 | 7 | 8 | 9 |
| 0 | IN | · | 1 | 1 | · | · | · | · | · | · | · |
| 1 | SC | $\text{int}_1$ | · | 1 | · | · | · | · | · | · | · |
| 2 | Thalamus | · | · | · | 1 | · | 1 | 1 | 1 | 1 | 1 |
| 3 | NRT | · | · | −1 | · | · | · | · | · | · | · |
| 4 | GPi/SNr | · | −1 | −1 | −1 | · | · | · | · | · | · |
| 5 | STN | · | · | · | · | 2 | · | 2 | · | · | 2 |
| 6 | GPe | · | · | · | −1/2 | −1/2 | −1/2 | · | −1/2 | −1/2 | · |
| 7 | Str-D2 | · | · | · | · | · | · | −1 | · | · | · |
| 8 | Str-D1 | · | · | · | · | −1/2 | · | −1/2 | · | · | · |
| 9 | CCortex | $\text{int}_2$ | 1/2 | 1 | 1/2 | · | 1/2 | · | 1/2 | 1/2 | · |

to the level of activation of the corresponding node #, as defined in Table I. For example, state $(1,1,0,1,0,0,0,0,1)^T$ corresponds to a network state characterized by activity in SC (node #1), Thalamus (node #2), GPi/SNr (node #4), and in CCortex (node #9). Then, state $(1,1,0,1,0,0,0,0,1)^T$ is represented by binary number "110100001," which corresponds to decimal number 417. The finite state automaton associated with the Boolean model of the basal ganglia-thalamocortical network is illustrated in Fig. 2(b). The numbers of the nodes are the decimal encodings of the binary numbers corresponding to the states that they represent [for instance, nodes 0 and 511 represent states $(0,0,0,0,0,0,0,0,0)^T$ and $(1,1,1,1,1,1,1,1,1)^T$, respectively]. The color of the edge from node $i$ to node $j$ of the graph is blue or red if and only if the network switches from state $i$ to state $j$ when receiving input 0 or 1, respectively. The cycles in the automaton correspond to the attractors of the network. Any modification in the connectivity pattern or in the values of the control parameters of the Boolean model would induce a corresponding modification of its corresponding automaton (cf. Sec. II A).

The simulation of the model is run following synchronous discrete time step updates of the state of all nodes. A consequence of the simplification of the physiological reality of the basal ganglia-thalamocortical circuit is the fact that we have left aside the differences in conduction delays between the various projections within the circuit. We may consider each time step as a time interval that includes the cumulative effects of axonal conduction delays, synaptic transmission, postsynaptic potential kinetics, and axosomatic integration necessary to reach threshold, if the activation—i.e., the depolarization of the cells—is large enough. We have also assumed the same dynamics for excitatory and inhibitory connections. On the basis of experimental data reported in the literature,[60,63–65] the order of magnitude of the time steps here should not be considered as time events lasting in the order of 4–10 ms and not 1 ms, as usually reported for spatiotemporal firing patterns.

### B. Neuronal excitability as a control parameter

In the absence of background activity and stochastic inputs, the whole network dynamics is deterministic. An input

pattern of activity provided only once at the beginning of the simulation may either evolve toward a silent network—no neurons are active—or toward a cyclic pattern of activity, if the activity is such to be self-sustained without external inputs, as illustrated elsewhere.[66] After some delay, a repeating input pattern of activity provokes an activity in the network that is necessarily going to repeat through the same sequence of states. For example, let us consider the basal ganglia-thalamocortical network (Fig. 2) with the topology described in Table I. The sensitivity to the control parameters is illustrated in Fig. 3. The same initial repeating pattern of activation (at the top of each panel) may lead to different dynamics as a function of a small perturbation in the threshold of excitability—i.e., a control parameter—[between Figs. 3(a) and 3(b)] or as a function of a small perturbation in the adjacency matrix—i.e., the network topology—[between Figs. 3(b) and 3(c)].

In the current framework, the neuronal excitability of the network corresponds to the *threshold* $\theta$ of activation for all Boolean units, since there is no other parameter controlling this feature. Note that a decrease or an increase in this threshold provokes the same effect as a global potentiation or global depression of the network's synaptic connections, respectively. For any $\theta \in \mathbb{R}$, the notation $\mathcal{N}_\theta$ refers to the basal ganglia-thalamocortical network of Fig. 2(a) with the adjacency matrix of Table I and with the threshold of its Boolean units being set to $\theta$. For each value of $\theta$ in the range $[0, 1.4]$ by steps of 0.1, we computed the entire list of attractors of network $\mathcal{N}_\theta$ (for this purpose, we first computed the automaton $\mathcal{A}_\theta$ associated with $\mathcal{N}_\theta$ and then computed the cycles of $\mathcal{A}_\theta$, as described in Sec. II A).

For $\theta = 0$, the only attractor of $\mathcal{N}_\theta$ is a single-point attractor corresponding to cycle $(511, 511)$. Node 511 encodes the network's state when all brain areas are active. Therefore, for $\theta = 0$, the threshold is so low that all elements of the circuit remain active once activated, irrespective of the input pattern of activity. This single-point attractor corresponds to a degenerate dynamics. For $\theta \in \{0.1, 0.2, 0.3, 0.4, 0.5\}$, the number of attractors of $\mathcal{N}_\theta$ is equal to 25, and this set of attractors is the same for any threshold within that interval of $\theta$ (cf. Table II). For $\theta \in \{0.6, 0.7, 0.8, 0.9, 1.0\}$, the number of attractors of $\mathcal{N}_\theta$ is 22, and this other set of attractors is the same for any threshold within that interval. These two sets of attractors are very different as they share only the degenerate single-point attractor corresponding to cycle $(0, 0)$. This degenerate attractor is the only attractor observed for any $\theta \geq 1.1$, because the threshold is set too high for any of the elements to be activated. The attractor dynamics of network $\mathcal{N}_\theta$ is therefore a piecewise constant function of $\theta$ with high discontinuity. The attractor dynamics of the network remains stable within specific ranges of threshold, but for certain specific values, the network switches from one dynamics to a very different one. In the present case, four distinct attractor dynamics have been observed.

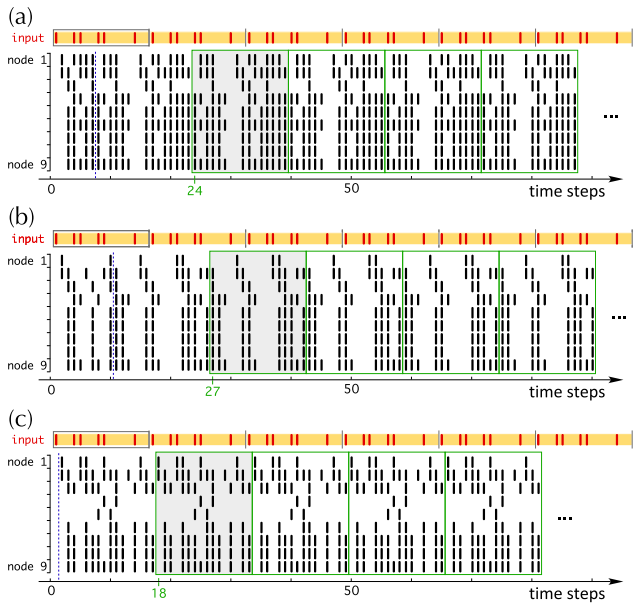


FIG. 3. Examples of raster displays showing different spatiotemporal patterns of activity in the basal ganglia-thalamocortical network of Fig. 2(a) associated with different dynamics produced by the same initial repeating pattern of activation. At the top of each panel, the series of repeating stimulation pulses, lasting 16 time steps, is labeled in red with yellow background. Dotted blue lines in each panel indicate the appearance of a repeating spatiotemporal pattern. For a comparison with the physiological model, the order of magnitude of the time steps here should not be considered in the order of 4–10 ms. (a) The rows of the rasters correspond to the nodes of the network with the same adjacency matrix as Table I and the threshold of excitability set $\theta = 0.5$. The spatiotemporal pattern (gray area) started to appear at time 8, with a cycle duration of 16 time steps, and then we considered the beginning of the repetition at time 24. (b) Identical network as panel (a) with the same initial pattern of activation. The only difference is the value of the threshold of excitability, $\theta = 0.6$. The spatiotemporal pattern (gray area) started to repeat at time 27, with a cycle duration of 16 time steps. (c) Identical threshold of excitability as panel (b) with the same initial pattern of activation. The network is the same (Table I) with a difference in just one synaptic weight, namely, $w_{2,5} = 0.9$ (i.e., Thalamus $\rightarrow$ STN) instead of its original value $w_{2,5} = 1.0$. The spatiotemporal pattern (gray area) started to repeat at time 18, with a cycle duration of 16 time steps.

### C. Effect of local connectivity

The *local connectivity*, as defined by the adjacency matrix of Table I, was kept fixed in the results presented so far. The effects of small changes in local connectivity on attractor dynamics of the basal ganglia-thalamocortical network are studied by introducing independent weight perturbations, by steps of 0.1 decrease or increase, of one non-interactive connection at a time and by computing the number of attractors as described in Sec. II A.

The results reported in Fig. 4 correspond to a network with threshold fixed at $\theta = 1.0$ and whose connection strengths were perturbed by 0.1. Each bar represents the number of attractors reached when a specific weight is decreased by 0.1 with respect to its reference value (Table I). The red line shows that in the absence of changes (i.e., the reference values), the number of attractors is equal to 22. All connection strengths of the adjacency matrix are labeled $w_{i,j}$, with $i$ being the source and $j$ the target area.

A decrease by 0.1 of $w_{2,5}$ (i.e., Thalamus $\rightarrow$ STN) triggers a switch to a dynamics of higher complexity with 143 distinct attractors. A similar decrease for $w_{6,5}$ (GPe $\rightarrow$ STN)

TABLE II. Attractors of $\mathcal{N}_\theta$ for the different values of $\theta$. The attractors are expressed as cycles of the automaton $\mathcal{A}_\theta$ (cf. Sec. II A). Nodes of $\mathcal{A}_\theta$ are numbers between 0 and 511 encoding the states of the network $\mathcal{N}_\theta$ (cf. Sec. III). For each cycle, the last node, being equal to the first one, is not mentioned.

| $\theta \in \{0.1, 0.2, 0.3, 0.4, 0.5\}$<br>25 attractors | $\theta \in \{0.6, 0.7, 0.8, 0.9, 1.0\}$<br>22 attractors |
|---|---|
| (0) | (0) |
| (0, 384, 223, 383, 41) | (0, 384, 223, 127, 33) |
| (0, 384, 223, 383, 425, 159, 511, 63, 41) | (0, 384, 223, 511, 63, 33) |
| (0, 384, 223, 383, 425, 159, 511, 447, 191, 63, 41) | (0, 384, 223, 511, 191, 63, 33) |
| (0, 384, 223, 383, 425, 415, 511, 63, 41) | (0, 384, 479, 255, 63, 33) |
| (0, 384, 223, 383, 425, 415, 511, 447, 191, 63, 41) | (0, 384, 479, 511, 63, 33) |
| (0, 384, 223, 511, 63, 41) | (0, 384, 479, 511, 191, 63, 33) |
| (0, 384, 223, 511, 447, 191, 63, 41) | (31, 161) |
| (0, 384, 479, 511, 63, 41) | (31, 417, 159, 255, 63, 161) |
| (0, 384, 479, 511, 447, 191, 63, 41) | (31, 417, 159, 511, 63, 161) |
| (41, 384, 223, 383) | (31, 417, 159, 511, 191, 63, 161) |
| (41, 384, 223, 383, 425, 159, 511, 63) | (33, 128, 95) |
| (41, 384, 223, 383, 425, 159, 511, 447, 191, 63) | (33, 128, 95, 417, 159, 255, 63) |
| (41, 384, 223, 383, 425, 415, 511, 63) | (33, 128, 95, 417, 159, 511, 63) |
| (41, 384, 223, 383, 425, 415, 511, 447, 191, 63) | (33, 128, 95, 417, 159, 511, 191, 63) |
| (41, 384, 223, 511, 63) | (33, 128, 479, 255, 63) |
| (41, 384, 223, 511, 447, 191, 63) | (33, 128, 479, 511, 63) |
| (41, 384, 479, 511, 63) | (33, 128, 479, 511, 191, 63) |
| (41, 384, 479, 511, 447, 191, 63) | (63, 161, 159, 255) |
| (63, 425, 159, 511) | (63, 161, 159, 511) |
| (63, 425, 159, 511, 447, 191) | (63, 161, 159, 511, 191) |
| (63, 425, 415, 511) | (191) |
| (63, 425, 415, 511, 447, 191) | |
| (191, 447) | |
| (447) | |

and $w_{9,5}$ (CCortex → STN) triggers a dynamics of high complexity with 65 distinct attractors. The common point to all these local connectivity modifications highlighted in Fig. 5(b) is that a decrease in activation, or an increase in depression, of node STN provokes an increase in the complexity of network dynamics. Conversely, a decrease in strength of either $w_{4,2}$ (SNR → Thalamus), $w_{5,4}$ (STN → SNR), $w_{6,4}$ (GPe → SNR), $w_{8,4}$ (Str-D1 → SNR), or $w_{9,2}$ (CCortex → Thalamus) provokes a decrease in complexity dynamics to as few as 5 or 8 distinct attractors. It is also interesting to note that a large number of local connections have little or no effect on the attractor dynamics of the network, as illustrated by the arrows highlighted in Fig. 5(a). Much larger positive or negative changes of these latter connections would still not change the attractor dynamics. Therefore, there exist paths in the network, here represented by the excitatory pathway "Thalamus → Str-D1 & Str-D2 ⇝ STN → CCortex → SC" which can be severely perturbed with little effect on the attractor regime of the network.

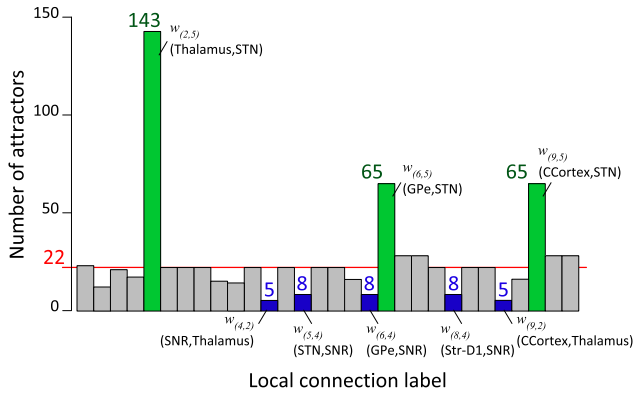


FIG. 4. Number of distinct attractors of network $\mathcal{N}_\theta$ with a fixed threshold $\theta = 1.0$ as a function of the decrease of each of its non-interactive weight by $-0.1$, one at a time. The red line represents the level of 22 of distinct attractors observed in the absence of any change with respect to the reference values of the adjacency matrix (Table I).

## IV. THE ROLE OF INTERACTIVITY

The output nodes of the basal ganglia-thalamocortical circuit are meant to send an efferent connection toward the effector nuclei associated with a motor and behavioral response. These output nodes have also a recurrent connection to the circuit via the links $\text{int}_1$ and $\text{int}_2$ [Figs. 2(a) and 5]. The information carried by these feedback connections is integrated with the external input, thus representing an interaction between the network and its environment. These so-called *interactive connections* are assumed to play a crucial role in the processing of information. The notation $\mathcal{N}_{\theta,\text{int}_1,\text{int}_2}$ refers to the network [Fig. 2(a)] whose threshold and strengths of interactive connections have been set to $\theta, \text{int}_1$, and $\text{int}_2$, respectively.

Figure 6 shows the number of attractors of $\mathcal{N}_{\theta,\text{int}_1,\text{int}_2}$ for threshold $\theta = 0.5$, and for the interactive connections $\text{int}_1$ and $\text{int}_2$ whose strength varied in the interval $[-1.5, 1.5]$ by steps of 0.1 (which means 961 overall tiles for this figure). Note that the attractor dynamics is a piecewise constant function

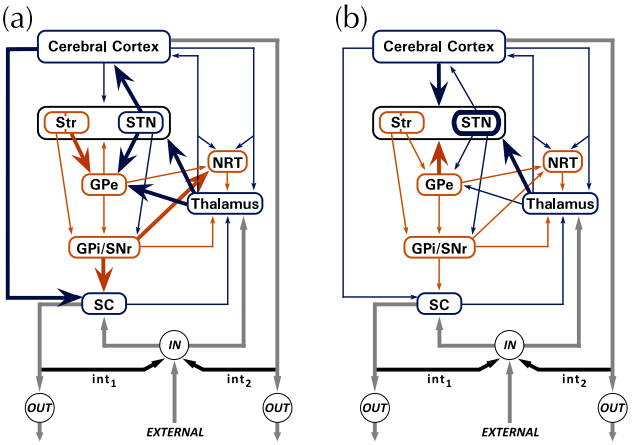


FIG. 5. Effect of *small decreases* in local connectivity strength on the attractor dynamics of the basal ganglia-thalamocortical network. Dark blue or orange arrows correspond to positive and negative weights, respectively. (a) The thick arrows highlight those connections whose small decreases do not affect the network's attractor dynamics. (b) A small decrease in connection strength of the thick arrows provokes a large increase in the number of attractors observed in the dynamics. Notice the key role played by node STN.

of $\text{int}_1$ and $\text{int}_2$ characterized by stable domains delimited by highly discontinuous boundaries. In this figure, we observed 10 domains corresponding to 10 different dynamics, i.e., with 1, 2, 3, 4, 6, 8, 9, 11, 21, and 25 distinct attractors. It is important to note that the same number of distinct attractors does not necessarily mean that the attractors are formed by the same sets of states. In the example of Fig. 6, we show that the

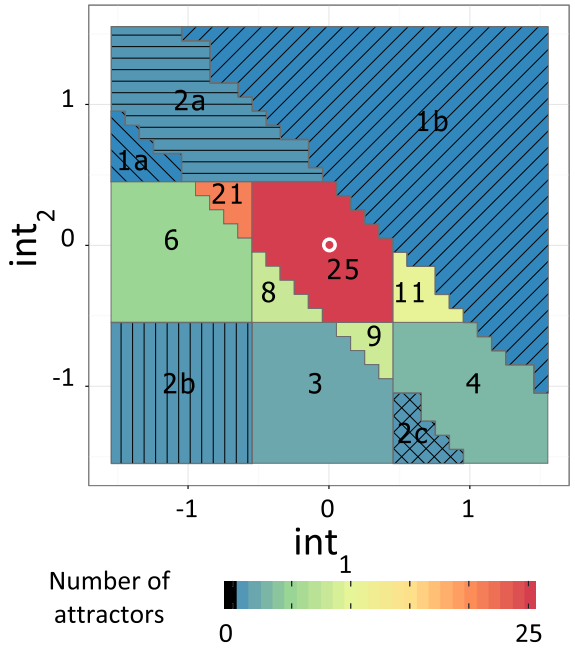


FIG. 6. Combined effect of the interactivity and the neuronal excitability on the attractor dynamics of the network $\mathcal{N}_{\theta,\text{int}_1,\text{int}_2}$ with threshold $\theta = 0.5$, and with the interactive weights $\text{int}_1$ and $\text{int}_2$ varying in the range $[-1.5, 1.5]$ by step of 0.1 along the $x$ and $y$ axes, respectively. The color scale corresponds to the number, indicated by a black label within the domain, of distinct attractors ranging from 1 (blue tiles) to 25 (red tiles). No interactivity, i.e., $\text{int}_1 = \text{int}_2 = 0$, is highlighted by a white circle at the center of the figure. Note that domains with the same color—i.e., 1a and 1b, and 2a, 2b, and 2c—are characterized by attractors comprising different set of states.

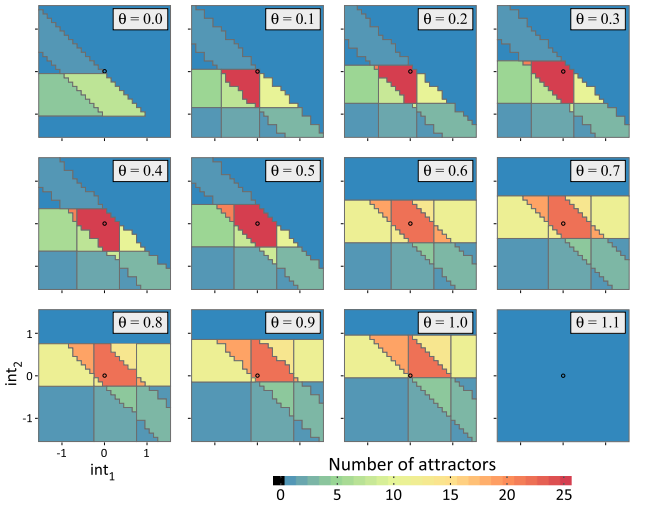


FIG. 7. The same figure as Fig. 6 illustrating the combined effect of the interactivity and the neuronal excitability on the attractor dynamics of the network. Each panel shows the number of attractors of the network $\mathcal{N}_{\theta,\text{int}_1,\text{int}_2}$ with a fixed value of threshold $\theta$ indicated in the corresponding legend. No interactivity, i.e., $\text{int}_1 = \text{int}_2 = 0$, is highlighted by a black circle in each panel.

domain with 1 attractor can be actually separated in two subdomains, labeled 1*a* and 1*b*, and the domain with 2 attractors into 2*a*, 2*b*, and 2*c*. We do not discuss further in this paper the additional complexity introduced by taking into account the subdomains with the same number of attractors. This is a matter of study we are currently undergoing and will be presented in a separate article in the near future.

Figure 7 extends the plot of Fig. 6 to the number of attractors of $\mathcal{N}_{\theta,\text{int}_1,\text{int}_2}$ for each value of the threshold $\theta$ between 0 and 1.1 by steps of 0.1. For $\theta = 0$, there are 4 different attractor dynamics with 1 ($n = 651$ tiles in Fig. 7), 2 ($n = 105$ tiles), 5 ($n = 105$ tiles), and 8 ($n = 100$ tiles) distinct attractors, depending on the values of the weights of interactive connections. For $\theta = 0.6$, we observed 10 domains, i.e., with 1, 2, 3, 4, 5, 11, 12, 13, 19, and 22 distinct attractors, which are only partially overlapping with the domains observed for $\theta = 0.5$. The smallest domains in Fig. 7, corresponding to 1 tile, were observed for $\theta = 0.2$, at point ($\text{int}_1 = 0.1$, $\text{int}_2 = -0.8$) triggering a dynamics with 9 attractors and at point ($-0.8$, 0.1) triggering 21 attractors. Also, for $\theta = 0.9$, we observed domains with just 1 tile, at point ($-0.1$, $-0.1$) triggering 13 attractors and at point (0.8, $-0.1$) triggering 19 attractors. Note that the point with coordinates $\text{int}_1 = \text{int}_2 = 0$, without any interactivity, generally lies near the boundary of the domain characterized by the single-point degenerate attractor with all units remaining indefinitely active. Therefore, a small amount of interactivity is sufficient to bring the network dynamics attracted into another domain with slightly more complexity. For $\theta = 1.1$, any combination of interactive connection strengths generated only 1 attractor domain, corresponding to the single-point degenerate attractor with all units remaining inactive because the threshold of activation is too high irrespective of any input pattern.

The modification of the strength of both the interactivity and local connectivity shows that attractor dynamics may be tuned in a fine way to switch between domains

characterized by different levels of complexity or to compensate each other and settle the network into stable attractor dynamics. We extend the previous notation such that $\mathcal{N}_{w_{i,j},\theta,\text{int}_1,\text{int}_2}$ refers to the number of attractors of the network of Fig. 2(a) whose threshold and strengths of interactive and local non-interactive connections $(i,j)$ have been set to $\theta, \text{int}_1, w_{i,j}$, respectively. Figure 8 shows $\mathcal{N}_{w_{i,j},\theta,\text{int}_1,\text{int}_2}$ with fixed threshold $\theta = 1.0$, interactive connection strengths $\text{int}_1, \text{int}_2$ varying between $-1.5$ and 1.5 by steps of 0.1 and non-interactive connection strengths weakened by $-0.1$ one at a time (with respect to the reference adjacency matrix of Table I).

In all panels, notice the existence of several domains with the same number of attractors. The diversity of the dynamics defined as the number of distinct domains of complexity might be considered as an additional feature. Both Figs. 8(e) and 8(f) are characterized by a diversity equal to 9, but the distribution of the complexity among the domains is slightly different and makes the difference between the two panels. Despite the similarity in the shape of their domains, Figs. 8(g) and 8(h) are characterized by a diversity including 8 and 10 different attractor dynamics, respectively. In Fig. 8(j), we observed the largest diversity in the attractor dynamics with 11 distinct domains and a maximum complexity equal to 65 different attractors. The highest complexity of 143 different attractors was observed in Fig. 8(k), which is characterized by a diversity of 9 domains. These results suggest that the interactivity may compensate small perturbations of local connectivity in terms of complexity (defined by the number of attractors).

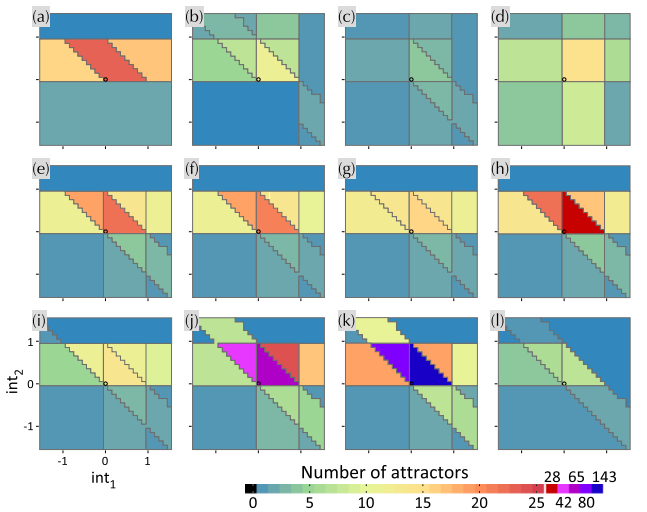


FIG. 8. Combined effect of the interactivity and the local connectivity on the attractors dynamics of the network. Each panel shows the number of distinct attractors with fixed threshold $\theta = 1.0$, one non-interactive connection strength decreased by $-0.1$ (with respect to the reference adjacency matrix, Table I) and the interactive weights $\text{int}_1$ and $\text{int}_2$ varying in the range $[-1.5, 1.5]$ by step of 0.1 along the $x$ and $y$ axes, respectively. The number of distinct attractors is continuously color coded between 1 (blue tiles) and 50 (red tiles), but the three largest values (i.e., 65, 80, and 143) have been color coded in a discontinuous scale. The white lines correspond to isoclines and delimit the domains of attractor dynamics. No interactivity, i.e., $\text{int}_1 = \text{int}_2 = 0$, is highlighted by a black circle in each panel. Dynamics after a decrease in input connections (a) $w_{0,1}$ and (b) $w_{0,2}$. The next panels show the effect of the decrease by $-0.1$ in the following local connections: (c) the same dynamics in either $w_{4,2}, w_{9,2}$; (d) $w_{2,9}$; (e) the same dynamics in either $w_{2,6}, w_{2,7}, w_{8,8}, w_{4,1}, w_{4,3}, w_{5,6}, w_{5,9}, w_{7,6}, w_{8,6}, w_{9,1}$; (f) $w_{1,2}$; (g) $w_{2,3}, w_{6,3}, w_{9,3}$; (h) $w_{6,7}, w_{6,8}, w_{9,7}, w_{9,8}$; (i) $w_{3,2}$; (j) $w_{6,5}, w_{9,5}$; (k) $w_{2,5}$; (l) $w_{5,4}, w_{6,4}, w_{8,4}$.

## V. ATTRACTOR DYNAMICS DEPENDENCY ON ADAPTIVE PLASTICITY OF LOCAL CONNECTIONS

We introduce a procedure to change the strength of a local connection by a STDP rule associated with the attractor dynamics. In addition to the timing between the activations of pre- and post-synaptic neurons, this new rule is based on an adaptive plasticity rate which modifies the connection strengths as a function of the successive attractor dynamics that the network encounters throughout its computational process. The rule is designed to shift network activity toward an increase in the complexity of attractor dynamics. More precisely, whenever the network receives some input stream, it produces successive spiking patterns that modify the synaptic weights according to the STDP. Hence, at each time step, the topology of the network—i.e., its adjacency matrix—has slightly changed, and the perturbations in the synaptic strengths provoked may affect the number of attractors of the network (as described in Sec. III C) at that very precise time step. In our procedure, we consider that these variations influence in turn the STDP rule itself. As a consequence, the network dynamics can stabilize in domains characterized by high complexity (i.e., with a large number of attractor dynamics), rather than switching between attractor dynamics of low complexity. The application of this procedure to the basal ganglia-thalamocortical network during its computational process is illustrated at the end of this section.

Formally, we consider the following adaptive STDP rule bounded by a definite weight interval $I = [I_1, I_2]$:

$$a_{ij}(t+1) = \begin{cases} I_1, \text{if } R < I_1, \\ R, \text{if } I_1 \leq R \leq I_2, \\ I_2, \text{if } R > I_2, \end{cases} \tag{3}$$

where

$$R = a_{ij}(t) + \lambda(t)\left\{x_i(t+1)x_j(t) - C[x_i(t)x_j(t+1)]\right\}, \tag{4}$$

and $x_i(t), x_j(t), x_i(t+1), x_j(t+1)$ are the activation values of neurons $i$ and $j$ at time $t$ and $j$ at times $t$ and $t+1$, respectively, $a_{ij}(t)$ and $a_{ij}(t+1)$ are the strength of the connections from $j$ to $i$ at time $t$ and $t+1$, respectively, $C$ is a constant modulating the weight decrease, and $\lambda(t)$ is the adaptive plasticity rate described below.

Let $n(t)$ be the number of attractors of the network at time $t$, and $n_{min}(t)$ and $n_{max}(t)$ be the minimum and maximum number of attractors that the network has encountered during the last $M$ time steps, for some constant $M > 0$:

$$\begin{aligned} n(t) &= \text{number of attractors of the network at time } t, \\ n_{min}(t) &= \min\{n(t') : \max(0, t-M) \leq t' \leq t\}, \\ n_{max}(t) &= \max\{n(t') : \max(0, t-M) \leq t' \leq t\}. \end{aligned}$$

The constant $M$ is called the *memory* of the network. It corresponds to the time window during which the network

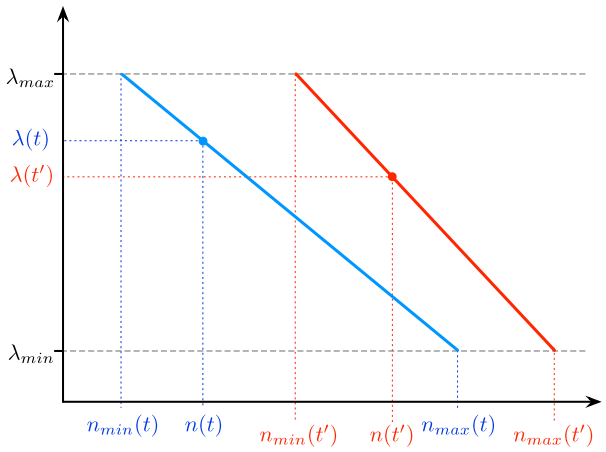


FIG. 9. Computation of the adaptive plasticity rate $\lambda(t)$ at two time steps $t$ (blue) and $t'$ (red). As time increases, the values $n_{min}(.)$ and $n_{max}(.)$ evolve along the $x$-axis. The interpolation lines vary in consequence. The current number of attractor $n(.)$ determines the current rate $\lambda(.)$.

"remembers" the minimum and maximum number of attractor that it has encountered.

The adaptive plasticity rate $\lambda(t)$ is computed as the linear interpolation between the two points $[n_{min}(t), \lambda_{max}]$ and $[n_{max}(t), \lambda_{min}]$, where $\lambda_{min}, \lambda_{max} \in \mathbb{R}$ are two bounds such that $\lambda_{min} < \lambda_{max}$. Formally, the rate $\lambda(t)$ is given by

$$\lambda(t) = \begin{cases} \lambda_{max} + [n(t) - n_{min}(t)] \dfrac{\lambda_{min} - \lambda_{max}}{n_{max}(t) - n_{min}(t)}, \\ \qquad \text{if } n_{min}(t) \neq n_{max}(t) \\ \lambda_{max} \quad \text{otherwise.} \end{cases} \tag{5}$$

The computation of $\lambda(t)$ is illustrated in Fig. 9. If $n(t) = n_{min}(t)$ [resp. $n(t) = n_{max}(t)$], it means that the current attractor dynamics of the network is at a minimal (resp. maximal) level. In this case, $\lambda(t) = \lambda_{max}$ [resp. $\lambda(t) = \lambda_{min}$]. Such large (resp. low) adaptive plasticity rate provokes large (resp. low) variations of the connection strengths with the aim of destabilizing (resp. stabilizing) the network's current dynamics. If $n_{min}(t) = n_{max}(t)$, the network dynamics has settled into a domain with the same complexity during the $K$ last steps. In this case, the new STDP rule sets $\lambda(t) = \lambda_{max}$ with the aim of perturbing the current dynamics and allowing the possibility to reach other states.

Note that $n_{min}(t)$ and $n_{max}(t)$ are functions of the memory $M$ [cf. Eq. (4)], so is $\lambda(t)$ [cf. Eq. (5)]. In this sense, the STDP rule is a function of the complexity of the attractor dynamics that the network encountered throughout its computational process. This adaptive feature is crucial to reach stable attractor dynamics of high complexity. Note that with memory $M = 1$, only the current number of attractors is considered. In this case, $n_{min}(t) = n_{max}(t)$ [cf. Eq. (4)]; hence, the adaptive plasticity rate $\lambda(t)$ is fixed to $\lambda_{max}$ for any time step $t$ [cf. Eq. (5)], and thus, the network dynamics is driven by a fixed-rate STDP rule. On the opposite, for any $M > 1$, the adaptive plasticity rate $\lambda(t)$ is time dependent, and therefore, the network dynamics is driven by the adaptive STDP rule.

In order to study the performance of the new STDP rule, we implemented Algorithm 1 for the Boolean network of Fig. 2 with a random input stream, and we recorded the

Algorithm 1. STDP-based adaptive weights procedure

**Input** : $A; B; \vec{c}; \lambda_{min}; \lambda_{max}; M; nb\_steps$
1: **// INITIALIZATION**
2: $A \leftarrow$ jitter($A$) `// random jitter of weight matrix A`
3: $X_0 \leftarrow$ zero_vector()
4: $\lambda \leftarrow \lambda_{max}$
5: attractors_list = [ ]
6: memory_list = [ ]
7: $t = 0$
8: **// SIMULATION**
9: **while** $t \leq nb\_steps$ **do**
10: $\vec{u} \leftarrow$ random_input() `// generate random input u`
11: $\vec{x_1} \leftarrow f_\theta(A \cdot \vec{x_0} + B \cdot \vec{u} + \vec{c})$
`// compute next state x_1 according to Eq. (2)`
12: $A \leftarrow$ stdp$(A, B, \vec{c}, \vec{x_0}, \vec{x_1}, \lambda)$
`// update weight matrix A according to Eq. (3)`
13: $\vec{x_0} \leftarrow \vec{x_1}$
14: $n \leftarrow$ nb_attractors$(A, B, \vec{c})$
`// compute nb of attractors of the net (Sec. II A)`
15: attractors_list.append($n$)
`// update list of attractors`
16: memory_list.append($n$) `// update memory`
17: **if** len(memory_list $\geq M$) **then**
18: memory_list.pop(0)
19: **end if**
20: $n_{min} \leftarrow$ min(memory_list)
21: $n_{max} \leftarrow$ max(memory_list)
22: $\lambda \leftarrow$ adaptive_rate$(n, n_{min}, n_{max}, \lambda_{min}, \lambda_{max})$
`// update rate lambda according to Eq. (5)`
23: $t \leftarrow t + 1$
24: **end while**
25: **return** attractors_list

sequence of attractor dynamics that the network encountered throughout its computational process.

At the beginning of each simulation, the strength $a_{ij}$ of each connection (Table I) was jittered by a random uniform noise $\epsilon_{ij} \sim \mathcal{U}(-0.025, 0.8)$ in order to lay within the weight interval $I_{ij} = [a_{ij} - 0.025; a_{ij} + 0.8]$ (line 2 of Algorithm 1). These bounds were chosen on the basis of an empirical analysis. We noticed that broader weight intervals bring the network dynamics to get trapped into connection weight configurations associated with a very low level of activity that does not allow any further update of the connection weights. The extreme values of adaptive plasticity rates were set to $\lambda_{min} = 0.002$ and $\lambda_{max} = 0.12$.

Simulations using the same random seed were run varying the values of the memory $M \in [1, 60, 120, 180, 240, 300]$. In this way, we ensure the same jittering process and input streams and allow for a direct analysis of the effect of varying the value of $M$. The results are displayed in Fig. 10. For $M = 1$—which represents a fixed-rate STDP rule— the sequences of attractor dynamics encountered by the networks are highly unstable. The largest complexity for $M = 1$ was equal to 66 and observed during intervals lasting 3 and 2 time steps in Figs. 10(a) and 10(c), respectively. In Fig. 10(b), the complexity level reached a value of 117 distinct attractors and lasted only 1 time step. In other simulation runs with $M = 1$ and within the first 300 time steps of simulation, we observed a level of complexity equal to 154, also lasting only 1 time

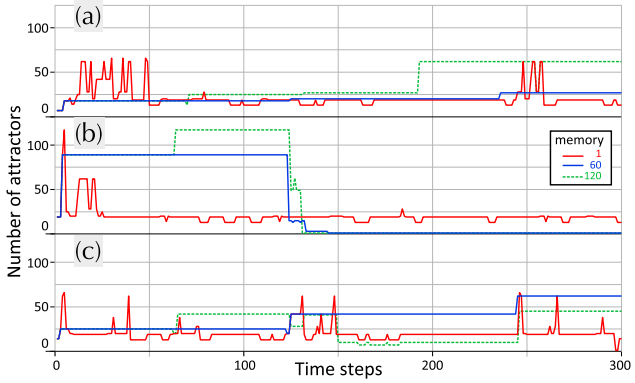


FIG. 10. Sequences of attractor dynamics encountered by the network during simulations of 300 time steps. At the beginning of each simulation run, the initial adjacency matrix of the connection strengths is randomly jittered. Then, at each time step, the network received a random input stream, the connection strengths are updated according to the STDP rule described by Eqs. (3)–(5), and the number of attractors is computed (see Sec. II A). Panels (a)–(c) show examples of curves for three different initial random seeds. In each panel, the same random seed is used with three different durations of the *memory* $M$ of the adaptive plasticity rate: $M = 1$, red curves; $M = 60$, blue curves; $M = 120$, dotted green curves.

step, but we cannot discard the existence of higher levels of complexity.

The same simulations with memory values set to $M = 60$ and $M = 120$ are also illustrated in Fig. 10. The results show that the larger the memory, the larger is the duration of sequences with the same dynamics. The median duration of stable sequences over many simulation runs with different random seeds tended to become equal to 8, 19, and 36 time steps with memory values of $M = 1$, $M = 60$, and $M = 120$, respectively. We observed also that the duration of a sequence with the largest value of complexity tended to be equal to

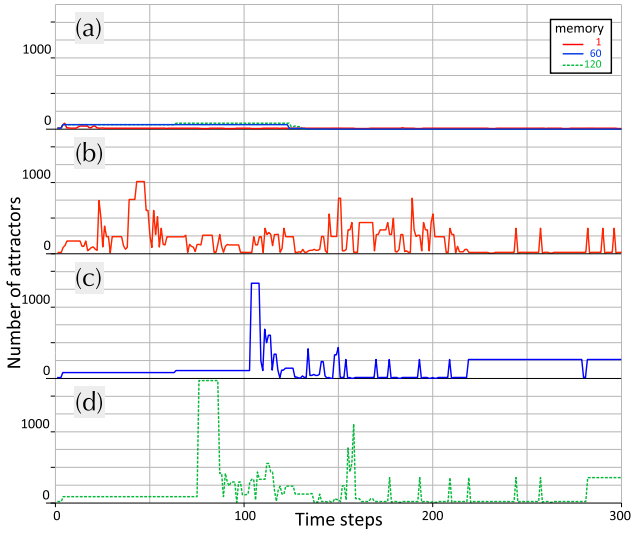


FIG. 11. Effect of the targeted adaptive STDP rule on the sequences of attractor dynamics encountered by the network during simulations of 300 time steps, with the same initial random seed in all panels. (a) The value of constant $C$ of weight decrease set to $C = 1$ for all connection weights of the network. Results for memory $M$ values equal to 1 (red curves), 60 (blue), and 120 (dotted green) time steps. This panel (a) is the same as Fig. 10(b) with a different scale. Panels (b)–(d) show the curves obtained with constant $C = 5$ for the three selected connections $w_{2,5}$, $w_{6,5}$, and $w_{9,5}$, and for memory values $M = 1$, $M = 60$, and $M = 120$, respectively.

the value $M$ of the memory. In particular, we observed, over a large set of simulation runs, complexity of 154 distinct attractors lasting 1 time step with $M = 1$, complexity 117 lasting 61 time steps with $M = 60$, and complexity 377 lasting 120 time steps with $M = 120$. These observations were confirmed by further simulations performed with memory values up to $M = 300$. The new adaptive STDP rule may bring the network dynamics to stabilize at high levels of complexity. However, the intervals of stable high complexity of attractor dynamics tended to last no more than the duration of the *memory* parameter. In some cases, the network dynamics could be driven toward very low complexity levels, where the network got trapped [e.g., Fig. 10(b), the dynamics falls to level 1 at time step $t = 131$, with $M = 60$, and at $t = 145$ with $M = 120$].

A remarkable high level of complexity was reached following a small decrease in connection strength (by $-0.1$ of its initial value) for three specific connections (i.e., $w_{2,5}$, $w_{6,5}$, and $w_{9,5}$, corresponding to projections Thalamus $\rightarrow$ STN, GPe $\rightarrow$ STN, and CCortex $\rightarrow$ STN, respectively; see Figs. 8(j) and 8(k). Therefore, it is rational to think that a targeted modification of these connections by adaptive plasticity might drive the network dynamics into a higher level of complexity. This hypothesis was explored by implementing a larger decrease adaptation update exclusively for those specific connection strengths [formally, the value of constant $C$ in Eq. (3) was set to $C = 5$ for connections $w_{2,5}$, $w_{6,5}$, and $w_{9,5}$, and the default value $C = 1$ was kept for any other connection]. A change of constant $C$ for only specific connections is referred to as *targeted adaptive STDP rule*.

In the absence of targeted adaptive STDP rule, Fig. 11(a) shows the same simulation run presented in Fig. 10(b), i.e., with peak complexities equal to 117 for $M = 1$ and $M = 60$, and to 89 for $M = 120$. In Figs. 11(b), 11(c), and 11(d), we note a huge increase in complexity due to the targeted adaptive STDP rule applied to connections $w_{2,5}$, $w_{6,5}$, and $w_{9,5}$ (with the same random seed and initial conditions). The level of complexity during the first 300 time steps increased to 1003 [Fig. 11(b)], 1335 [Fig. 11(c)], and 1735 distinct attractors [Fig. 11(d)] with $M = 1$, $M = 60$, and $M = 120$, respectively. The outcome of applying the targeted adaptive STDP rule was very variable and depended on particular initial conditions. In a different simulation run, we observed a complexity level increasing to 6126 distinct attractors, but in other runs, the complexity of the attractor dynamics stabilized to lower levels.

## VI. DISCUSSION

Synchronous discrete-time first-order recurrent neural networks made up of classical McCulloch and Pitts cells[67] represent the classic framework for the implementation of Boolean neural systems with the advantage of a complete analysis of the attractor dynamics of the networks. In this framework, the attractors of the networks correspond to the cycles of their corresponding automata and thus can be computed explicitly and exhaustively. We studied the attractor dynamics of a Boolean model of the basal ganglia-thalamocortical network as a function of properties related to

the whole network, such as neuronal excitability and modulation of the strength of its local connectivity. The complexity of attractor dynamics computed here is determined by the number of distinct attractors of the network and their stability throughout the computational processes.

In the absence of changes in synaptic strengths, we have provided evidence that the attractor dynamics can be adjusted by the feedback connections to the sensory input in order to maintain the dynamics into basins of high levels of complexity. In a similar way, given constrained feedback connectivity, the network dynamics can be adjusted to move toward stable basins of high complexity levels by adjusting whole network properties. Experimental evidence exists for decades that the absence of one feature in neuronal dynamics relevant to spike-triggering may be compensated for by the presence of another.[3] In our study, we considered a Boolean model of the basal ganglia-thalamocortical network,[32] a circuit formed by several parallel and segregated circuits involving different areas of the brain linking sensorimotor information processing with emotion and memory.[60] In the real world, the neuromodulatory inputs to the basal ganglia-thalamocortical circuit affect the overall excitability of the network in relation to sensory processing, arousal, sleep-waking cycle, and cognitive evaluation of reward and aversion.[68–72]. Therefore, the general conjecture that the neural dynamics "may guide activity-dependent learning processes in such a way that synaptic strengths, firing thresholds, the physical connections between neurons, and the size of the network are automatically set in an optimal, interrelated fashion"[45] is supported by this study. Our results are also in agreement with the hypothesis that global attractors would be an indivisible set of circuit structures generated by membrane and synapse activation and silencing that are associated with the firing-rate dynamics specific of developmental stages.[16,73,74].

Our results showed that decreases in selected connection strengths in the basal ganglia-thalamocortical network provoke the strongest influence in shifting the attractor dynamics to extreme high levels. Dependence of both the induction and expression of STDP on the type of postsynaptic interneurons has been experimentally observed to contributing differential processing by corticostriatal projections storage of information in local cortical circuits.[75–77] This complexity highlights the extraordinary potential of inhibitory STDP as a major regulatory mechanism, controlled by neuromodulators (such as dopaminergic inputs in the basal ganglia) for higher cognitive functions.[78–81] The projections producing the main effect in our results are converging on the node corresponding to the subthalamic nucleus. A decrease in activation, or an increase in depression, of node STN provokes an increase in the complexity level of attractor dynamics. The particular location of the STN node in the circuit topology is such that it is highly sensitive to the Excitatory and Inhibitory (E/I) balance. The inhibitory hub of the basal ganglia, GPe, inhibits STN, while it receives excitatory inputs from the cerebral cortex. The delicate interplay of these combined projections determines the faith of the pattern of activity in STN and, eventually, of the complexity of the attractor dynamics of the whole circuit.

The STN is implicated in the limbic/cognitive functions of the basal ganglia,[82] and it plays a key role in controlling the balance between funneling information via the hyperdirect cortico-subthalamic pathway and parallel processing through the parallel cortico-basal ganglia-subthalamic pathways, both of which are necessary for selected motor behaviors.[83] Indeed, depression of STN activity by deep brain stimulation is considered the major therapeutic intervention in order to decrease the symptoms produced by Parkinson's disease[84,85] and absence epilepsy seizure.[86] Combining modulation of membrane excitability and gain control of feedback inhibition enables thalamic circuits to finely tune the gating of activity from sensory organs to the cortex and switch between oscillatory activity—periodic orbits in the limit cycles—and wakeful unawareness—chaotic dynamics—either by direct excitation of an arousal nucleus or by inhibition of a sleep-promoting centre in the basal forebrain.[87–90] Hence, converging wealth of evidence emphasizes that spatially and temporally structured inhibition via recurrent networks is likely to play a key role in sequence generation.[91,92]

We have introduced a new connectivity strength adaptive rule based on the timing between the activation of pre- and the post-synaptic neurons, inspired by the STDP rule[56–58] and by the successive attractor dynamics that the network encounters throughout its computation. Then, it was not surprising to observe that, when the rule applies to all the connections in the same way, the stabilization of the attractor dynamics depends on the memory parameter of the adaptivity rule, i.e., akin of a membrane time constant. Initial conditions, as usually in nonlinear dynamical systems, are extremely important, and several simulation runs could not reach the highest levels of complexity. The new adaptive STDP rule implements a twofold evolving process: the connection strengths evolve according to the STDP rule, but the STDP rule itself also evolves over time according to the "attractor history" of the network dynamics, by modifying its rate according to Eq. (5). These interwoven evolving processes emphasize the effect of time-dependency, which is crucial to our study. A time-dependency rule modifies significantly the computational power of Boolean recurrent neural networks and brings it to a super-Turing level, irrespective of its rational value, that is to the level achieved with static real-weighted synaptic connections.[93,94] It is necessary to remind that the time scale of the model studied here does not correspond to the 0.1–1 ms discrete time scales, which are often reported in many simulations. A model closer to the physiological reality should incorporate additional data related to the latencies and axonal delays of the connections between the brain areas of the model. The literature is extremely vast, but the experimental values depend on the species being investigated (mostly rats and primates) and the animal preparation (e.g., behaving, unanesthetized, the type of anesthetics). We can estimate that 1 time step in the current model of the basal ganglia-thalamocortical circuit might correspond to a physiological interval in the order of 4–10 ms.

The overall idea presented here is that an adaptive STDP rule modifies the network's topology—by changing its synaptic weights—in order to stabilize into an architecture characterized by a large number of attractors. These numerous attractors could then be made available to the network for the implementation of numerous cognitive processes (e.g.,

efficient memory processes). The larger the number of attractors at disposal, the larger the possibilities to enable complex cognitive processes. We observe that targeted STDP rule, applied to a selected subset of the connections, is able to increase the complexity of attractor dynamics by few orders of magnitude, consistent with the hypothesis that dynamic network reorganization requires modifications of selected neuronal gains, revealing a mechanism that networks may use to selectively transfer neural response properties.[95] The attractor dynamics adaptive plasticity rule modifying the local connection strengths is able to drive the computational process of network dynamics toward high levels of complexity, but the rule itself is not able to maintain an attractor dynamics of high complexity for an interval lasting more than the memory of the network.

It is important to consider that the presence of a multistable system according to perceptual alternation (implemented by interactivity) allows transitions between attractor states that might represent an advantage for the neural system, as more favorable functional outcomes could appear under certain conditions. On the other hand, the stabilization processes of the attractor dynamics also represent an advantage for the implementation of robust neural functionalities. These considerations could suggest that the dynamics of the network is confronted to seek a compromise between the advantage of a chaotic itinerancy and the stability of its attractors. It is necessary to extend our study in order to include a reinforcement process and memory consolidation, that is, a process adapting the memory parameter in targeted connections, because no learning occurs without, or independent of, reward.[80,96] The inclusion of a reward circuit in future studies would introduce a conditional multistability, capable to let emerge robust, though flexible, attractor dynamics, in agreement with the latest experimental studies.[97]

In conclusion, our results suggest that multiple parameters controlling the attractor dynamics of boolean recurrent networks can compensate one another in order to shift or to maintain the attractor dynamics at certain levels of complexity. By either potentiating or depressing targeted connection strengths, the networks could either switch from one attractor dynamics to a very different one or, on the contrary, settle themselves into stable domains that remain invariant under perturbations of small intensity.

## ACKNOWLEDGMENTS

The authors acknowledge the partial support by the Swiss National Science Foundation [NSF(CH)] (Grant No. IZK0Z2 161582).

[1]J. P. Segundo, "Nonlinear dynamics of point process systems and data," Int. J. Bifurcat. Chaos **13**, 2035–2116 (2003).
[2]J. P. Segundo, G. P. Moore, L. J. Stensaas, and T. H. Bullock, "Sensitivity of neurones in Aplysia to temporal pattern of arriving impulses," J. Exp. Biol. **40**, 643–667 (1963), available at http://jeb.biologists.org/content/40/4/643.full.pdf.
[3]H. L. Bryant and J. P. Segundo, "Spike initiation by transmembrane current: A white-noise analysis," J. Physiol. **260**, 279–314 (1976).
[4]M. Abeles, *Local Cortical Circuits. An Electrophysiological Study*, Studies of Brain Function Vol. 6 (Springer-Verlag, Berlin, 1982).
[5]A. E. P. Villa and M. Abeles, "Evidence for spatiotemporal firing patterns within the auditory thalamus of the cat," Brain Res. **509**, 325–327 (1990).
[6]A. E. P. Villa and J. M. Fuster, "Temporal correlates of information processing during visual short-term memory," Neuroreport **3**, 113–116 (1992).
[7]M. Abeles, H. Bergman, E. Margalit, and E. Vaadia, "Spatiotemporal firing patterns in the frontal cortex of behaving monkeys," J. Neurophysiol. **70**, 1629–1638 (1993).
[8]I. V. Tetko and A. E. P. Villa, "A pattern grouping algorithm for analysis of spatiotemporal patterns in neuronal spike trains. 2. Application to simultaneous single unit recordings," J. Neurosci. Methods **105**, 15–24 (2001).
[9]P. E. Rapp, I. D. Zimmerman, A. M. Albano, G. C. Deguzman, and N. N. Greenbaun, "Dynamics of spontaneous neural activity in the simian motor cortex: The dimension of chaotic neurons," Phys. Lett. A **110**, 335–338 (1985).
[10]G. J. Mpitsos, R. M. Burton, Jr., H. C. Creech, and S. O. Soinila, "Evidence for chaos in spike trains of neurons that generate rhythmic motor patterns," Brain Res. Bull. **21**, 529–538 (1988).
[11]A. Celletti and A. E. P. Villa, "Low-dimensional chaotic attractors in the rat brain," Biol. Cybern. **74**, 387–393 (1996).
[12]A. Celletti, V. M. B. Lorenzana, and A. E. P. Villa, "Correlation dimension for paired discrete time series," J. Stat. Phys. **89**, 877–884 (1997).
[13]A. Babloyantz, J. M. Salazar, and C. Nicolis, "Evidence of chaotic dynamics of brain activity during the sleep cycle," Phys. Lett. A **111**, 152–155 (1985).
[14]E. Başar, "Chaotic dynamics and resonance phenomena in brain function: Progress, perspectives, and thoughts," in *Chaos in Brain Function*, edited by E. Başar (Springer, Berlin, 1990), pp. 1–30.
[15]Y. Asai and A. E. P. Villa, "Reconstruction of underlying nonlinear deterministic dynamics embedded in noisy spike trains," J. Biol. Phys. **34**, 325–340 (2008).
[16]J. Iglesias and A. E. P. Villa, "Recurrent spatiotemporal firing patterns in large spiking neural networks with ontogenetic and epigenetic processes," J. Physiol. Paris **104**, 137–146 (2010).
[17]W. Little, "The existence of persistent states in the brain," Math. Biosci. **19**, 101–120 (1974).
[18]M. I. Rabinovich, P. Varona, A. I. Selverston, and H. D. I. Abarbanel, "Dynamical principles in neuroscience," Rev. Mod. Phys. **78**, 1213–1265 (2006).
[19]J. J. Knierim and K. Zhang, "Attractor dynamics of spatially correlated neural activity in the limbic system," Annu. Rev. Neurosci. **35**, 267–285 (2012).
[20]J. J. Hopfield, "Neural networks and physical systems with emergent collective computational abilities," Proc. Natl. Acad. Sci. U.S.A. **79**, 2554–2558 (1982).
[21]D. J. Amit, *Modeling Brain Function: The World of Attractor Neural Networks*, 2nd ed. (Cambridge University Press, 1992).
[22]G. Schöner, "Timing, clocks, and dynamical systems," Brain Cogn. **48**, 31–51 (2002).
[23]S. Thorpe, A. Delorme, and R. Van Rullen, "Spike-based strategies for rapid processing," Neural. Netw. **14**, 715–725 (2001).
[24]E. D. Adrian and Y. Zotterman, "The impulses produced by sensory nerve-endings: Part II. The response of a single end-organ," J. Physiol. **61**, 151–171 (1926).
[25]V. B. Mountcastle, G. F. Poggio, and G. Werner, "The relation of thalamic cell response to peripheral stimuli varied over an intensive continuum," J. Neurophysiol. **26**, 807–834 (1963).
[26]W. Bialek, R. de Ruytervan Steveninck, F. Rieke, and D. Warland, *Spikes: Exploring the Neural Code* (MIT Press, 1999).
[27]S. Grossberg, "Pavlovian pattern learning by nonlinear neural networks," Proc. Natl. Acad. Sci. U.S.A. **68**, 828–831 (1971).
[28]T. Kohonen, "Self-organized formation of topologically correct feature maps," Biol. Cybern. **43**, 59–69 (1982).
[29]P. J. Werbos, "Generalization of backpropagation with application to a recurrent gas market model," Neural. Netw. **1**, 339–356 (1988).
[30]V. Del Prete, L. Martignon, and A. E. P. Villa, "Detection of syntonies between multiple spike trains using a coarse-grain binarization of spike count distributions," Network **15**, 13–28 (2004).
[31]J. Cabessa and A. E. P. Villa, "A hierarchical classification of first-order recurrent neural networks," Chin. J. Physiol. **53**, 407–416 (2010).
[32]J. Cabessa and A. E. P. Villa, "An attractor-based complexity measurement for boolean recurrent neural networks," PLoS One **9**, e94204 (2014).
[33]J. J. Hopfield and D. W. Tank, "Computing with neural circuits: A model," Science **233**, 625–633 (1986).

[34]H. T. Siegelmann and E. D. Sontag, "Analog computation via neural networks," Theor. Comput. Sci. **131**, 331–360 (1994).
[35]H. Siegelmann and E. Sontag, "On the computational power of neural nets," J. Comput. Syst. Sci. **50**, 132–150 (1995).
[36]J. Cabessa and A. E. Villa, "The expressive power of analog recurrent neural networks on infinite input streams," Theor. Comput. Sci. **436**, 23–34 (2012).
[37]J. Cabessa and J. Duparc, "Expressive power of nondeterministic recurrent neural networks in terms of their attractor dynamics," Int. J. Unconv. Comput. **12**, 25–50 (2016), available at http://www.oldcitypublishing.com/pdf/7589.
[38]J. Cabessa and A. E. P. Villa, "Expressive power of first-order recurrent neural networks determined by their attractor dynamics," J. Comput. Syst. Sci. **82**, 1232–1250 (2016).
[39]F. Pasemann and N. Stollenwerk, "Attractor switching by neural control of chaotic neurodynamics," Network **9**, 549–561 (1998).
[40]M. Cencini, M. Falcioni, D. Vergni, and A. Vulpiani, "Macroscopic chaos in globally coupled maps," Phys. D **130**, 58–72 (1999).
[41]S. Wu, K. Hamaguchi, and S.-I. Amari, "Dynamics and computation of continuous attractors," Neural. Comput. **20**, 994–1025 (2008).
[42]K. Kaneko, "From globally coupled maps to complex-systems biology," Chaos **25**, 097608 (2015).
[43]S.-I. Amari, "Learning patterns and pattern sequences by self-organizing nets of threshold elements," IEEE Trans. Comput. **100**, 1197–1206 (1972).
[44]G. Palm, *Neural Assemblies: An Alternative Approach to Artificial Intelligence*, Studies of Brain Function Vol. 7 (Springer-Verlag, Berlin, 1982).
[45]G. J. Mpitsos, "Attractors: Architects of Network Organization?," Brain Behav. Evol. **55**, 256–277 (2000).
[46]K. Kaneko and I. Tsuda, *Complex Systems Chaos and Beyond: A Constructive Approach with Applications in Life Sciences* (Springer, Berlin, 2001).
[47]K. Kaneko and I. Tsuda, "Chaotic itinerancy," Chaos **13**, 926–936 (2003).
[48]S. C. Kleene, "Representation of events in nerve nets and finite automata," in *Automata Studies*, edited by C. Shannon and J. McCarthy (Princeton University Press, Princeton, NJ, 1956), pp. 3–41.
[49]M. L. Minsky, *Computation: Finite and Infinite Machines* (Prentice-Hall, Inc., Englewood Cliffs, NJ, 1967).
[50]J. Cabessa and H. T. Siegelmann, "The super-Turing computational power of plastic recurrent neural networks," Int. J. Neural. Syst. **24**, 1450029 (2014).
[51]D. J. Amit and S. Fusi, "Learning in neural networks with material synapses," Neural. Comput. **6**, 957–982 (1994).
[52]W. C. Abraham and A. Robins, "Memory retention—the synaptic stability versus plasticity dilemma," Trends Neurosci. **28**, 73–78 (2005).
[53]H. T. Siegelmann and L. E. Holzman, "Neuronal integration of dynamic sources: Bayesian learning and Bayesian inference," Chaos **20**, 037112 (2010).
[54]A. Knoblauch, G. Palm, and F. T. Sommer, "Memory capacities for synaptic and structural plasticity," Neural Comput. **22**, 289–341 (2010).
[55]D. Malagarriga, A. E. P. Villa, J. Garcia-Ojalvo, and A. J. Pons, "Consistency of heterogeneous synchronization patterns in complex weighted networks," Chaos **27**, 031102 (2017).
[56]C. C. Bell, V. Z. Han, Y. Sugawara, and K. Grant, "Synaptic plasticity in a cerebellum-like structure depends on temporal order," Nature **387**, 278–281 (1997).
[57]H. Markram, J. Lübke, M. Frotscher, and B. Sakmann, "Regulation of synaptic efficacy by coincidence of postsynaptic APs and EPSPs," Science **275**, 213–215 (1997).
[58]D. E. Feldman, "The spike-timing dependence of plasticity," Neuron **75**, 556–571 (2012).
[59]J. Cabessa and A. E. P. Villa, "Attractor dynamics driven by interactivity in boolean recurrent neural networks," Lecture Notes Comp. Sci. **9886**, 115–122 (2016).
[60]*Handbook of Basal Ganglia Structure and Function*, 2nd ed., edited by H. Steiner and K. Y. Tseng, Handbook of Behavioral Neuroscience Vol. 24 (Elsevier, 2017), pp. i–xxiii, pp. 1–1012.
[61]M. L. Perreault, A. Hasbi, B. F. O'Dowd, and S. R. George, "The dopamine D1-D2 receptor heteromer in striatal medium spiny neurons: Evidence for a third distinct neuronal pathway in basal ganglia," Front. Neuroanat. **5**, 31 (2011).
[62]F. Sato, M. Parent, M. Levesque, and A. Parent, "Axonal branching pattern of neurons of the subthalamic nucleus in primates," J. Comp. Neurol. **424**, 142–152 (2000).
[63]E. D. Lumer, G. M. Edelman, and G. Tononi, "Neural dynamics in a model of the thalamocortical system. I. Layers, loops and the emergence of fast synchronous rhythms," Cereb. Cortex **7**, 207–227 (1997).
[64]M. Salami, C. Itami, T. Tsumoto, and F. Kimura, "Change of conduction velocity by regional myelination yields constant latency irrespective of distance between thalamus and cortex," Proc. Natl. Acad. Sci. U.S.A. **100**, 6174–6179 (2003).
[65]C. R. Stoelzel, Y. Bereshpolova, J.-M. Alonso, and H. A. Swadlow, "Axonal conduction delays, brain state, and corticogeniculate communication," J. Neurosci. **37**, 6342–6358 (2017).
[66]A. Villa and I. Tetko, "Spatio-temporal patterns of activity controlled by system parameters in a simulated thalamo-cortical neural network," in *Supercomputing in Brain Research: From Tomography to Neural Networks*, edited by H. Herrmann, D. Wolf, and E. Poppel (World Scientific, 1995) pp. 379–388.
[67]W. S. McCulloch and W. Pitts, "A logical calculus of the ideas immanent in nervous activity," Bull. Math. Biophys. **5**, 115–133 (1943).
[68]S. L. Foote and J. H. Morrison, "Extrathalamic modulation of cortical function," Annu. Rev. Neurosci. **10**, 67–95 (1987).
[69]D. A. McCormick and H. C. Pape, "Noradrenergic and serotonergic modulation of a hyperpolarization-activated cation current in thalamic relay neurones," J. Physiol. **431**, 319–342 (1990).
[70]A. E. P. Villa, I. V. Tetko, P. Dutoit, and G. Vantini, "Non-linear cortico-cortical interactions modulated by cholinergic afferences from the rat basal forebrain," Biosystems **58**, 219–228 (2000).
[71]B. E. Jones, "From waking to sleeping: Neuronal and chemical substrates," Trends Pharmacol. Sci. **26**, 578–586 (2005).
[72]S. Spiga, A. Lintas, and M. Diana, "Altered mesolimbic dopamine system in THC dependence," Curr. Neuropharmacol. **9**, 200–204 (2011).
[73]T. S. Turova and A. E. P. Villa, "On a phase diagram for random neural networks with embedded spike timing dependent plasticity," Biosystems **89**, 280–286 (2007).
[74]Y. Baram, "Developmental metaplasticity in neural circuit codes of firing and structure," Neural. Netw. **85**, 182–196 (2017).
[75]J.-T. Lu, C.-y. Li, J.-P. Zhao, M.-m. Poo, and X.-h. Zhang, "Spike-timing-dependent plasticity of neocortical excitatory synapses on inhibitory interneurons depends on target cell type," J. Neurosci. **27**, 9711–9720 (2007).
[76]E. Fino and L. Venance, "Spike-timing dependent plasticity in the striatum," Front. Synaptic. Neurosci. **2**, 6 (2010).
[77]X. Ji, S. Saha, J. Kolpakova, M. Guildford, A. R. Tapper, and G. E. Martin, "Dopamine receptors differentially control binge alcohol drinking-mediated synaptic plasticity of the core nucleus accumbens direct and indirect pathways," J. Neurosci. **37**, 5463–5474 (2017).
[78]S. M. Vogt and U. G. Hofmann, "Neuromodulation of STDP through short-term changes in firing causality," Cogn. Neurodyn. **6**, 353–366 (2012).
[79]T. P. Vogels, R. C. Froemke, N. Doyon, M. Gilson, J. S. Haas, R. Liu, A. Maffei, P. Miller, C. J. Wierenga, M. A. Woodin, F. Zenke, and H. Sprekeler, "Inhibitory synaptic plasticity: Spike timing-dependence and putative network function," Front. Neural. Circuits **7**, 119 (2013).
[80]R. R. Kerr, D. B. Grayden, D. A. Thomas, M. Gilson, and A. N. Burkitt, "Coexistence of reward and unsupervised learning during the operant conditioning of neural firing rates," PLoS One **9**, e87123 (2014).
[81]M.-L. Wang and J.-S. Wang, "Dynamical balance between excitation and inhibition of feedback neural circuit via inhibitory synaptic plasticity," Acta. Phys. Sin. **64**, 108701 (2015).
[82]N. Maurice, J. M. Deniau, A. Menetrey, J. Glowinski, and A. M. Thierry, "Prefrontal cortex-basal ganglia circuits in the rat: Involvement of ventral pallidum and subthalamic nucleus," Synapse **29**, 363–370 (1998).
[83]A. Lintas, I. G. Silkis, L. Albéri, and A. E. Villa, "Dopamine deficiency increases synchronized activity in the rat subthalamic nucleus," Brain Res. **1434**, 142–151 (2012).
[84]W. D. Hutchison, R. J. Allan, H. Opitz, R. Levy, J. O. Dostrovsky, A. E. Lang, and A. M. Lozano, "Neurophysiological identification of the subthalamic nucleus in surgery for Parkinson's disease," Ann. Neurol. **44**, 622–628 (1998).
[85]F. Njap, J. C. Claussen, A. Moser, and U. G. Hofmann, "Modeling effect of GABAergic current in a basal ganglia computational model," Cogn. Neurodyn. **6**, 333–341 (2012).

[86]B. Hu, Y. Guo, X. Zou, J. Dong, L. Pan, M. Yu, Z. Yang, C. Zhou, Z. Cheng, W. Tang, and H. Sun, "Controlling mechanism of absence seizures by deep brain stimulus applied on subthalamic nucleus," Cogn. Neurodyn. **12**, 103–119 (2018).

[87]A. E. P. Villa, I. V. Tetko, P. Dutoit, Y. De Ribaupierre, and F. De Ribaupierre, "Corticofugal modulation of functional connectivity within the auditory thalamus of rat, guinea pig and cat revealed by cooling deactivation," J. Neurosci. Methods **86**, 161–178 (1999).

[88]G. Le Masson, S. Renaud-Le Masson, D. Debay, and T. Bal, "Feedback inhibition controls spike transfer in hybrid thalamic circuits," Nature **417**, 854–858 (2002).

[89]C. K. E. Moll, A. Sharott, W. Hamel, A. Münchau, C. Buhmann, U. Hidding, S. Zittel, M. Westphal, D. Müller, and A. K. Engel, "Waking up the brain: A case study of stimulation-induced wakeful unawareness during anaesthesia," Prog. Brain Res. **177**, 125–145 (2009).

[90]L. Albéri, A. Lintas, R. Kretz, B. Schwaller, and A. E. Villa, "The calcium-binding protein parvalbumin modulates the firing properties of the reticular thalamic nucleus bursting neurons," J. Neurophysiol. **109**, 2827–2841 (2013).

[91]J. Cannon, N. Kopell, T. Gardner, and J. Markowitz, "Neural sequence generation using spatiotemporal patterns of isnhibition," PLoS Comput. Biol. **11**, e1004581 (2015).

[92]K. Rajan, C. D. Harvey, and D. W. Tank, "Recurrent network models of sequence generation and memsory," Neuron **90**, 128–142 (2016).

[93]J. Cabessa and H. T. Siegelmann, "Evolving recurrent neural networks are super-Turing," in *2011 International Joint Conference on Neural Networks (IJCNN)* (IEEE, 2011), pp. 3200–3206.

[94]J. Cabessa and A. E. P. Villa, "Recurrent neural networks and super-Turing interactive computation," Springer Series in Bio-/Neuroinformatics, **4**, 1–29 (2015).

[95]J. M. Young, W. J. Waleszczyk, C. Wang, M. B. Calford, B. Dreher, and K. Obermayer, "Cortical reorganization consistent with spike timing—but not correlation-dependent plasticity," Nat. Neurosci. **10**, 887–895 (2007).

[96]J. G. Mikhael and R. Bogacz, "Learning reward uncertainty in the basal gasnglia," PLoS Comput. Biol. **12**, e1005062 (2016).

[97]G. Rodriguez, M. Sarazin, A. Clemente, S. Holden, J. T. Paz, and B. Delord, "Conditional bistability, a generic cellular mnemonic mechanism for robust and flexible working memory computations," J. Neurosci. (2018).